ACS APPLIED MATERIALS & INTERFACES

www.acsami.org

Research Article

Tuning Local Order in Starch Nanoparticles Exploiting Nonsolvency with "Green" Solvents

Andrea Casini, Margherita Casagli, Giovanna Poggi, David Chelazzi,* and Piero Baglioni

Cite This: *ACS Appl. Mater. Interfaces* 2024, 16, 21185−21196

Read Online

ACCESS | Metrics & More | Article Recommendations | Supporting Information

ABSTRACT: Starch is a renewable biopolymer that can be sourced from agricultural waste and used to produce nanoparticles (SNPs). In particular, amorphous SNPs have potential application in numerous fields, including the consolidation of weakened paintings in the cultural heritage preservation. Starch dissolution followed by nanoprecipitation in nonsolvents is an advantageous synthetic route, but new methodologies are needed to feasibly control the physicochemical properties of the SNPs. Here, we explored nanoprecipitation by nonsolvency using a set of "green" solvents to obtain amorphous SNPs, rather than starch nanocrystals already reported in the literature. The effect of the nonsolvent on the ordering of polymer chains in the obtained SNPs was studied. The recovery of local order (e.g., isolated V-type helices) after dissolution was shown to depend on the type of solvents used in the dissolution and precipitation steps, while long-range order (extended arrays of helices) is lost. Aqueous dispersions of the SNPs provided effective consolidation of powdery painted layers, showing that the selection of particle synthetic routes can be dictated by sustainability and scalability criteria. These "green" formulations are candidates as new consolidants in art preservation, and the possibility of tuning local order in amorphous starch assemblies might also impact fields like food chemistry, pharmaceutics, and nanocomposites, where SNPs with tunable amorphousness are more advantageous than nanocrystals.

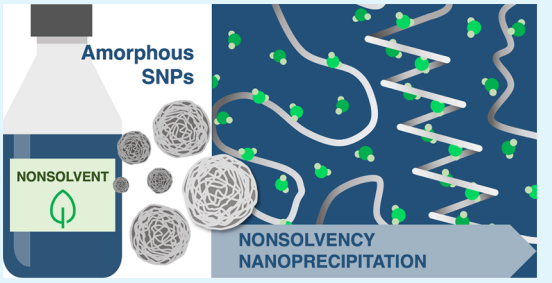

KEYWORDS: *starch nanoparticles, soft matter, nanoprecipitation, green solvents, nonsolvency, paintings consolidation, cultural heritage conservation*

INTRODUCTION

Over the past decade, green chemistry has grown to become an imperative in the development of advanced materials in several scientific and technological fields[1] spanning from food chemistry, cosmetics, catalysis, tissue engineering, detergency, drug-delivery, and pharmaceutics, up to recent applications of high socio-economic importance such as the use of colloids and soft matter for the remedial and preventive conservation of cultural heritage assets.[2−13] In these frameworks, biopolymers or solvents selected according to existing standards (e.g., the European REACH Regulation 1907/2006[14] − Registration, Evaluation, Authorisation and Restriction of Chemicals) represent ideal starting materials for processing and synthetic routes, as they can be used in new and safer approaches that comply with the need of reducing potential threats to human health or the environment.[15]

Biomass materials contain natural polymers with structural strength and stability[16] and have been used since ancient times. Starch, being a renewable and available biopolymer that can be sourced from agricultural and food wastes, is an optimal candidate in the formulation of advanced colloids and soft matter in multiple fields.[17,18] In particular, amorphous starch nanoparticles (SNPs) can be advantageous over starch nanocrystals, since they have faster reactivity and dynamics useful in applications such as drug-delivery,[19] food chemistry,[20] adhesives/consolidants,[21] and composites.[22] Research has focused on the formulation of starch nanoparticles (SNPs) using several methods, mainly grouped as acid hydrolysis (also coupled with enzymatic debranching), milling, gamma irradiation, electro spraying, high-pressure homogenization, ultrasonication, and nanoprecipitation in nonsolvents.[23,24] Among these, nanoprecipitation is advantageous since it does not rely on concentrated acids or high energy input and can show larger yields than enzymolysis.[21,25] However, current methodologies for the nonsolvent precipitation of amorphous SNPs are still in their infancy, and the use of different green solvents and methodologies to tune the physicochemical characteristics of the obtained particles (e.g., size, shape, and crystallinity vs amorphousness) has not yet been explored.

Recently, we demonstrated an approach where granular Jin Shofu wheat starch is dissolved in aqueous potassium

Received: February 20, 2024
Revised: April 2, 2024
Accepted: April 4, 2024
Published: April 13, 2024

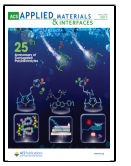

hydroxide (KOH) and nanoprecipitated in ethanol, obtaining amorphous SNPs that can be swollen in water or water−ethanol blends to yield nanogels.[21] Jin Shofu is a highly purified gluten-removed starch with advantageous characteristics: it can form films with ideal mechanical properties, and its low gelatinization temperature likely favors its disassembly in alkali to give low molecular weight polymer chains, which are able to reassemble upon exposition to the nonsolvent. The absence of gluten (which contains ethanol-soluble gliadin) also contributes to nanoprecipitation in ethanol. The obtained SNPs and nanogels formulations proved to be effective consolidants for paintings, rebuilding cohesion and adhesion of weakly bound pigments representative of those frequently met in the conservation of modern/contemporary canvas paintings.[21] These works can exhibit matte and powdery painted layers following aging and degradation, as in masterpieces by Edward Munch and Ernst Ludwig Kirchner. The new approach is alternative to solutions of bulk starch or synthetic adhesives, traditionally employed by painting conservators, which all involve aesthetic alterations (bulk starch forms glossy superficial films) or chemical degradation (development of acids by synthetic adhesives).[21,26]

We noticed that precipitation in ethanol produced SNPs with highly disordered polymer chain networks, which was ascribed both to the use of aqueous KOH (that contains structure-breaking ionic species) and to the nonsolvent effect of ethanol that might induce strongly abrupt assembly of the dissolved starch chains surrounded by the alcohol, preventing the formation of ordered domains.[21] This led to the hypothesis that the degree of order in the SNP polymer networks could be controlled by playing on the mutual chemical affinity of starch, solvent, and nonsolvent phases. This paper thoroughly investigates nonsolvency effects considering for the first time different synthetic routes, where we used either aqueous KOH or dimethyl sulfoxide (DMSO) to dissolve Jin Shofu starch, and a set of "green" nonsolvents for the nanoprecipitation step. The selection of solvents/nonsolvents was made according to the state-of-the-art literature on their safety and ecotoxicological impact based on current industrial and academic classifications. The compounds were also selected to cover a range of physicochemical parameters (dielectric constant, dipole moment, solubility parameters, ability to donate hydrogen bonds). The SNPs obtained with different routes were systematically characterized with a setup of techniques including X-ray diffraction and scattering and infrared spectroscopy, studying structural variations in the starch particles. Finally, the formulations were assessed in the consolidation of poorly bound painted layers mimicking degraded canvas/easel paintings of modern/contemporary production.

This approach allowed evaluating the overall sustainability of the formulations, matching sustainability and low ecotoxicological impact in their synthetic approach with their efficacy in the consolidation of weak painted layers. In addition, the collected results provide a basis for applicative research on SNPs, as in principle the degree of order in the nanoparticles can affect the optical and mechanical properties of starch films/gels to be used in several fields, as well as their resistance to attack by microorganisms.[17,18] Starch nanoparticles are known to be surface active and can be used as emulsifiers in food chemistry, cosmetics, and pharmaceutical products, for instance, employing nanostarch to stabilize Pickering emulsions.[17,27] The particles can also be used as encapsulation systems where the presence of ordered structures is crucial, like in starch-phenolic single helix inclusion complexes facilitated by the hydrophobic effect (e.g., hydrophobic cavities in V-type helices can entrap guest molecules) or weaker complexes driven by hydrogen bonds.[28,29] V-type helices are also involved in the formation of complexes between amylose and lipids as fat replacers in the food industry,[30] where the structure of the nanoparticles affects the digestibility and organoleptic tastes of the final product.[31] In nanocapsules, the internal morphology and the presence of strongly hydrated/swollen shells are relevant factors for biological and biomedical applications.[21,32] For instance, partly crystalline starch has been used to decorate microgels or form hybrids with poly(*N*-isopropylacrylamide), achieving better biocompatibility, while microgel monolayers can stabilize emulsions by interaction with hard colloids at the air−water interface.[32] Finally, local order is expected to affect the reactivity of SNP fillers in bioplastics, e.g., disordered particles could release reactive species to promote plastic photodegradation during irradiation.[33]

EXPERIMENTAL SECTION

Materials. The Jin Shofu wheat starch paste used for this study was supplied by Paper Nao (Tokyo, Japan). Starch was dissolved using ultrapure water Millipore MilliRO-6 Milli-Q gradient system (resistivity > 18 MΩ cm) with potassium hydroxide (KOH ≥ 86%, for analysis, pellets, Fluka), or dimethyl sulfoxide (DMSO, purity ≥ 99%, Sigma-Aldrich). For precipitation in nonsolvent, the following solvents were used: ethanol absolute anhydrous (EtOH, purity ≥ 99.9%, Carlo Erba), dimethyl carbonate (DMC, purity ≥ 99.9%, Sigma- Aldrich), *t*-butanol (*t*-But, purity ≥ 99.5%, Sigma-Aldrich), 2-butanol (2-But, purity ≥ 99.9%, Sigma-Aldrich), methyl ethyl ketone (MEK, purity ≥ 99.0%, Sigma-Aldrich), 2-propanol (2-Prop, purity ≥ 99.5%, Sigma-Aldrich), acetone (ACE, purity ≥ 99.5%, Sigma-Aldrich), propylene carbonate (PC, purity 99.0%, Sigma-Aldrich). SNPs were washed with denatured ethanol (denEtOH, purity ≥ 99.2%, Carlo Erba). The ultramarine blue pigment used for the preparation of modelized paint layers was provided by Zecchi (Florence, Italy).

Starch Nanoparticle (SNP) Synthesis. Starch nanoparticles were obtained through alkali or DMSO treatment of Jin Shofu starch followed by nonsolvent precipitation. Dissolution of starch in KOH (0.1 M) and nanoprecipitation in nonsolvents were carried out as detailed previously[21] but using water/ethanol blends or other nonsolvents besides ethanol. The ethanol contents in the blends were 25, 50, and 75% v/v. Dissolution of starch in DMSO (1% w/v) was carried out by mixing Jin Shofu starch powder in pure solvent. The dispersion was heated under vigorous stirring at 80 °C for 30 min to promote the dissolution of the native starch, resulting in an opalescent and homogeneous phase. The dissolved starch was then cooled to room temperature and added dropwise in the nonsolvent with a fixed solvent/nonsolvent ratio of 1/10 under constant stirring (1300 rpm). The water−ethanol nonsolvent blends had alcohol concentrations of 25, 50, and 75% v/v. The other nonsolvent phases comprised pure, nonblended solvents, e.g., ethanol, dimethyl carbonate, *t*-butanol, 2-butanol, methyl ethyl ketone, 2-propanol, acetone, and propylene carbonate. In all cases, a solvent/nonsolvent ratio of 1/10 v/v was used. The list and abbreviations of all the SNPs prepared for this study is shown in Table 1.

Physico-Chemical Characterization of the SNPs. Dynamic light scattering measurements (DLS) on 1 g/L SNPs water dispersions were carried out using a 90Plus particle size analyzer (Brookhaven Instruments), with incident 659 nm laser light radiation and collection at 90°. To obtain the particle size distributions from the measured autocorrelation functions, the CONTIN program was used (based on the original work by Provencher[34]), and the results were reported as intensity plots. Each specimen was analyzed at

https://doi.org/10.1021/acsami.4c02858
ACS Appl. Mater. Interfaces 2024, 16, 21185−21196

Table 1. SNP Samples Abbreviations, Along with Solvent and Nonsolvent Phases Used for Each Sample

sample	solvent	nonsolvent
$EtOH_{K50}$	potassium hydroxide in water (0.1 M)	ethanol:water (50:50 v/v %)
$EtOH_{K75}$	potassium hydroxide in water (0.1 M)	ethanol:water (75:25 v/v %)
$EtOH_{K100}$	potassium hydroxide in water (0.1 M)	ethanol
$EtOH_{D25}$	dimethyl sulfoxide	ethanol:water (25:75 v/v %)
$EtOH_{D50}$	dimethyl sulfoxide	ethanol:water (50:50 v/v %)
$EtOH_{D75}$	dimethyl sulfoxide	ethanol:water (75:25 v/v %)
$EtOH_{D100}$	dimethyl sulfoxide	ethanol
DMC_{D100}	dimethyl sulfoxide	dimethyl carbonate
t-But_{D100}	dimethyl sulfoxide	*t*-butanol
2-But_{D100}	dimethyl sulfoxide	2-butanol
MEK_{D100}	dimethyl sulfoxide	methyl ethyl ketone
2-$Prop_{D100}$	dimethyl sulfoxide	2-propanol
ACE_{D100}	dimethyl sulfoxide	acetone
PC_{D100}	dimethyl sulfoxide	propylene carbonate

constant temperature of 25 °C, and three independent measurements were taken, each consisting of 10 runs.

SEM analysis of dried SNPs was performed with a field emission gun scanning electron microscope SIGMA (FEG-SEM, Carl Zeiss Microscopy GmbH, Germany), using an acceleration potential of 3 kV and a 3.9 mm working distance. The SEM images of the dried SNPs after nanoprecipitation were analyzed with MorphoLibJ "distance transform watershed" method,[35,36] a collection of image processing methods based on mathematical morphology for ImageJ.[35] The images were converted to 8-bit format and binarized with an automatically calculated average threshold. Then, they were compared with the original 8-bit grayscale images using a cross-correlation analysis plug-in created by Chiga and Syverud,[37] following the same parameters as in Casini et al.[21] The binarized image with the highest values of correlation (R) and determination (R^2) coefficients was selected as the most accurate and used for further analysis. To avoid the influence of particle aggregates, at least three different regions of each SEM image were chosen for binarization and analysis, and the MorphoLibJ method was applied to identify individual particles. The diameters of the segmented areas (identified particles), resulting from this procedure, were then measured. To ensure reproducibility, three independent SEM images were analyzed for each SNP formulation, measuring about 100 particles in each image.

Scanning transmission electron microscopy (STEM) images were acquired on SNP water dispersions using a TESCAN GAIA 3 FIB/SEM system equipped with a STEM detector, operating at an accelerating voltage of 30 kV. The samples were prepared by dropping SNPs dispersed in water (1 g/L) on a carbon holey film placed on a 300 mesh Cu grid, followed by solvent evaporation at room temperature.

Attenuated total reflectance Fourier transform infrared spectroscopy (ATR-FTIR) was carried out on dried SNPs using a Thermo Nicolet Nexus 870 spectrometer equipped with a liquid-nitrogen-cooled HgCdTe detector and a single reflection diamond crystal ATR unit. Spectra were recorded in the 4000−650 cm^{-1} range, acquiring 128 scans with a spectral resolution of 2 cm^{-1}. Spectral band deconvolution of the 1190−880 cm^{-1} region was carried out with the multipeak fitting package of the Igor Pro software, version 9 (WaveMetrics, Inc.), using 9 Gaussian components and full widths at half-maximum (fwhm) of max 20 cm^{-1}. The components' wavenumbers were taken from the literature,[21,38,39] and the positions of bands were constrained within 5 cm^{-1}.

X-ray diffractometry (XRD) on SNPs was carried out using a Bruker New D8 Da Vinci diffractometer (radiation at Cu Kα1 = 1.54056 Å, 40 kV × 40 mA), equipped with a Bruker LYNXEYE-XE detector and a secondary monochromator. Data were collected in the 2θ range of 5−50°, with a slide of 0.6 mm, 2.5° soller slit configuration, step size of 0.02°, and time per step of 57.2 s. Deconvolution of diffractograms was carried out with the multipeak fitting package of the Igor Pro software, version 9 (WaveMetrics, Inc.), using 4 Gaussian components taken from the literature,[40,41] and constraining the bands position within 1° and the fwhm at max 5°.

Wide-angle X-ray scattering (WAXS) measurements were conducted on dried SNPs utilizing a Xeuss 3.0 HR instrument (Xenocs, Grenoble, France) equipped with an EIGER2R (1 M model) hybrid pixel photon counting detector (Dectris Ltd., Baden, Switzerland), featuring 1028 × 1062 pixels with dimensions of 75 × 75 μm^2. The X-ray beam wavelength employed was λ = 1.542 Å. The calibration of the sample-to-detector distance was executed employing silver behenate (d = 58.38 Å)[42] and lanthanum hexaboride (d = 4.15 Å).[43] The experiments were conducted under vacuum conditions to mitigate air scattering effects, with a sample-to-detector distance of 60 mm, enabling the exploration of a scattering vector range (q) from 0.0178 to 2.7287 $Å^{-1}$, where $q = (4\pi/\lambda)\sin\theta$ and 2θ represents the scattering angle. Powders were encapsulated within sealed demountable cells utilizing Kapton foils as windows. Absolute scattering intensities (in mm^{-1}) were determined by employing glassy carbon as a secondary standard. The 1D azimuthally averaged scattering profiles were processed by subtracting the scattering intensity from an empty holder. Data reduction and normalization were performed utilizing XSACT (X-ray Scattering Analysis and Calculation Tool, Xenocs, France).

Preparation and Treatment of Aged Painting Mock-Ups. Painting mock-ups were prepared by mixing ultramarine blue powder with deionized water (1:75, w/w) under constant stirring. The obtained paste was applied on a glass slide without any binder to simulate aged/degraded paintings with poor cohesion and adhesion onto the support. The mock-ups were dried in an oven at 60 °C (20% RH) overnight and then exposed to seven freeze−thaw cycles (−20 °C for 2 h and 60 °C at 20% RH for 2 h, for each cycle), producing highly powdery painted surfaces mimicking degraded canvas/easel painted layers of the modern/contemporary production. The aged painted layers were treated with SNP dispersions (5 g/L, in water): mock-ups of 2.5 × 5 cm^2 (≃1 mm thick) were treated by three spray applications (1 mL each).

Characterization of the Treated Paint Mock-Ups. The consolidation effect of the SNPs on the aged painting mock-ups was assessed using an in-house protocol described in detail elsewhere.[21] Essentially, the surfaces of paint mock-ups were sampled in a controlled and reproducible way, using a standardized sampler with a fiberglass filter that is put in contact with the aged painted layers (either before or after treatment with SNPs). Then, the amount of pigment removed by sampling was measured semiquantitatively by acquiring macrophotographs of the filter and binarizing the images with selected algorithms. The percentage of black pixels was measured and averaged over the selected images, and the final value directly yielded the pigment relative coverage (%) on the filter surface. The photographs were collected using a Canon EOS 5D Mark II Full Frame DSLR camera equipped with a Sigma 105 mm f/2.8 EX macro lens, with a light setup of 45° on both sides for reducing shadow formation on the surface of the filters. Image processing, binarization, and quantitative evaluation were carried out using GIMP (GNU Image Manipulation Program), ImageJ software, and a cross-correlation analysis plugin developed by Chinga et al., as previously detailed.[21,37]

RESULTS AND DISCUSSION

The first goal in our study was to implement a sustainable procedure for the dissolution of starch and its nanoprecipitation. Therefore, we classified a pool of solvents and nonsolvents according to their safety, sustainability and ecotoxicological impact based on current industrial and academic classifications found in the literature.[14,15,44,45] Solvents are

https://doi.org/10.1021/acsami.4c02858
ACS Appl. Mater. Interfaces 2024, 16, 21185−21196

Figure 1. Graphical representation of the global score that averages, for each starch solvent and nonsolvent considered in the present study, the "green" scores provided by industrial and academic institutions. Nonsolvents also include blends of water and ethanol. The global scores were translated in colors ranging from deep red (lower end) to yellow (average values) and up to deep green (high end), as shown by the ranking scale on the bottom.

Table 2. Physico-Chemical Properties of Nonsolvents (Series a, b, and c) and Solvents for the SNP Nanoprecipitation, Including the Hansen Partial Solubility Parameters, Namely, δ_d (Energy from Dispersion Forces between Molecules), δ_p (Dipolar Intermolecular Forces), and δ_h (Hydrogen Bonds), the Total (Hildebrand) Solubility Parameter δ_T, Dielectric Constant (ε), Dipole Moment (μ), the Solvent−Nonsolvent Solubility Parameter ($\Delta_{\delta S\text{-}NS}$), and the Solvent−Nonsolvent Interaction Parameter ($\chi_{S\text{-}NS}$)[a]

nonsolvent phase	ε	δ_d (MPa$^{1/2}$)	δ_p (MPa$^{1/2}$)	δ_h (MPa$^{1/2}$)	δ_T (MPa$^{1/2}$)	$\Delta\delta_{S\text{-}NS}$	$\chi_{S\text{-}NS}$	μ
(a) DMSO as Solvent; EtOH/H_2O as Nonsolvent								
EtOH:H_2O 100:0 v/v %	25.0	15.8	8.8	19.4	26.5	12.2	0.001	1.7
EtOH:H_2O 75:25 v/v %	35.7	15.8	10.6	25.1	31.5	16.2	0.532	
EtOH:H_2O 50:50 v/v %	47.7	15.7	12.4	30.9	36.8	21.3	2.200	
EtOH:H_2O 25:75 v/v %	64.5	15.7	14.4	36.6	42.4	26.6	2.905	
(b) KOH in H_20 (0.1M) as Solvent; EtOH/H_2O as Nonsolvent								
EtOH:H_2O 100:0 v/v %	25.0	15.8	8.8	19.4	26.5	24.0	10.704	1.7
EtOH:H_2O 75:25 v/v %	35.7	15.8	10.6	25.1	31.5	18.0	6.113	
EtOH:H_2O 50:50 v/v %	47.7	15.7	12.4	30.9	36.8	12.0	2.605	
(c) DMSO as Solvent; Pure "Green" Solvents as Nonsolvents								
DMC	3.1	17.4	9.6	3.90	20.3	9.3	1.401	0.2
t-But	12.5	15.2	5.1	14.70	21.7	12.6	0.935	1.3
2-But	16.6	15.8	5.7	14.50	22.2	11.8	0.746	1.4
MEK	18.5	16.0	9.0	5.10	19.1	9.3	2.100	2.8
2-Prop	19.3	15.8	6.1	16.40	23.6	12.3	0.296	1.6
ACE	20.5	15.5	10.5	7.00	20.0	7.3	1.337	2.7
EtOH	25.0	15.8	8.8	19.40	26.5	12.2	0.001	1.7
PC	64.9	20.0	18.0	4.10	27.2	6.5	0.010	4.9

solvent phase	ε	δ_d (MPa$^{1/2}$)	δ_p (MPa$^{1/2}$)	δ_h (MPa$^{1/2}$)	δ_T (MPa$^{1/2}$)	$\Delta\delta_{S\text{-}NS}$	$\chi_{S\text{-}NS}$	
DMSO	47.1	18.4	16.4	10.2	26.7			4.0
H_2O	78.4	15.6	16.0	42.3	47.8			1.9

[a] δ_T, $\Delta_{\delta S\text{-}NS}$, and $\chi_{S\text{-}NS}$ are calculated as detailed in the SI.

generally marked with scores based on the Innovative Medicines Initiative (IMI)−CHEM21, which use the most recent and stringent combination of SH&E criteria (Safety, Health, and Environment, taken from REACh and Safety Data

https://doi.org/10.1021/acsami.4c02858
ACS Appl. Mater. Interfaces 2024, 16, 21185−21196

Sheets). Other evaluations found in the literature include scores from the American Chemical Society's Green Chemistry Institute Pharmaceutical Roundtable (ACS GCI GCI-PR), as well as classifications and assessment updates provided by independent researchers.[14,44,45] Overall, the scores provided by each academic and industrial institution include parameters such as hazard and risk codes, legal exposure limits, and energy consumption and are expressed as colors, where a red flag indicates a highly hazardous solvent (major issues), yellow a problematic one (some issues), and green a recommended solvent (few or no issues).

Here, we calculated a global score for each chemical, which weighs all of the scores given to it by different institutions. First, we assigned numerical values of 1 to red flags, 2 to yellow flags, and 3 to green flags. The sum was then divided by the total number of score entries given to each chemical by all of the considered institutions, using two decimal digits for the result. We chose to ignore "unclassified" entries in the global score evaluation. For instance, 2-propanol has 0 red flags, 0 yellow flags, 6 green flags, and 1 "unclassified" entry, yielding a global score of 3.00. Finally, the global score of each chemical was translated in color ranging from deep red (lower end) to yellow (average values) up to deep green (high end) using nine color steps. In the case of the KOH solution (0.1M), the scores of water and pure KOH were averaged to yield the final value.

In Figure 1, we show a visual synthetic representation of the global scores (color scale) for the solvents that we evaluated in the present study.

All the selected compounds exhibit at least ∼10% (w/w) solubility in water, a required feature since some mutual miscibility between the solvent used for starch dissolution and the nonsolvent is necessary to achieve nanoprecipitation.[46] In addition, these compounds cover a range of different physicochemical properties (see Table 2), such as the dielectric constant, dipole moment, solubility parameters, and ability to donate hydrogen bonds. These parameters are expected to regulate the complex interplay of physicochemical interactions taking place between solvent and nonsolvent, and solvent/nonsolvent and starch chains, which in principle can produce different shape, size distribution, and structure of the SNPs.

Based on our classification, the selected nonsolvents show acceptable "green" scores. For starch dissolution, DMSO is less harmful than aqueous solutions of KOH (0.1 M), and it can be considered as less harmful than other approaches used for SNPs formulation, e.g., high volumes of concentrated acid.

Even though in principle some extraction procedures could be necessary to remove solvent or KOH residues from the final SNPs formulation, both approaches are significantly less expensive and more sustainable than using elevated pressure/temperature or systems with higher pH to dissolve starch. It must also be noticed that, according to the literature, the use of DMSO produces lesser alteration of the starch original molecular weight than alkaline environments.[21] In addition, we verified in preliminary trials that, when the KOH solution is used to dissolve starch, no nanoprecipitation occurred in the selected nonsolvents except for ethanol and water/ethanol blends, while dissolution in DMSO allowed nanoprecipitation in a wide spectrum of green solvents with different properties.

While Jin Shofu starch dissolved in KOH or DMSO is stable in water, the exposure to water/ethanol blends produced the precipitation of nanoparticles, except in the case of dissolution in KOH and exposure to a 75:25 (v/v) water/ethanol blend. Likewise, when the ethanol content is reduced to 5% of the nonsolvent blend, no precipitation is obtained regardless of the dissolution solvent.

DLS analysis (see Table 3) showed that, after dissolution in KOH or DMSO, precipitation in the water/ethanol blends,

Table 3. DLS Data of the Nanoparticle Aqueous Dispersions[a]

intensity diameter (nm)					
precipitation in water/ethanol blends			precipitation in neat nonsolvents		
$ETOH_{K100}$	129	±10	$t\text{-But}_{D100}$	176	±18
$EtOH_{K75}$	99	±9	2-But_{D100}	261	±11
$ETOH_{K50}$	126	±18	2-Prop_{D100}	193	±9
$ETOH_{D100}$	173	±16	MEK_{D100}	211	±2
$EtOH_{D75}$	138	±19	AC_{D100}	228	±5
$ETOH_{D50}$	141	±14	DMC_{D100}	183	±12
$EtOH_{D25}$	146	±12	PC_{D100}	180	±11

[a]The particles were obtained after nanoprecipitation of starch solutions in different nonsolvents. The dispersion nomenclature follows Table 1 (examples of the autocorrelation functions obtained for the dispersions are shown in Figure S1c).

and dispersion in water, the formulations contain objects with sizes of ca. 100−170 nm. These size values are comparable with those reported in the literature for starch nanoparticles precipitated using 1% (w/vol) starch content in the dissolution step.[47] SEM and TEM analysis of the dried particles right after nanoprecipitation (see Figure S1a,b), showed particles with sizes ca. 40−50 nm and small clusters of ca. 150−300 nm including few particles, compatible with the objects' sizes obtained by DLS on the particles aqueous dispersions.

Using dissolution in DMSO, the particles' size decreases slightly when the ethanol content in the nonsolvent is reduced from 100% to lower values. Previously, changing the affinity between the solvent and nonsolvent phases was in some cases reported to affect the particles' size by influencing the diffusion of the nonsolvent into the solvent.[48]

Structural information on the starch chains assembled in SNPs was first gained by ATR-FTIR and spectral deconvolution, analyzing trends in the ratios of starch absorptions at ca. 1000, 1020, and 1050 cm^{-1} (see Figure 2, and Figures S2−S7). These bands are assigned to C−O−H vibrations in the polymer. In addition, they have been associated with short-range H-bonding between starch chains (1000 cm^{-1}; molecular interactions, as in isolated V-type starch helices), to amorphous chain networks (1020 cm^{-1}), and to long-range order H-bonded networks (1050 cm^{-1}, arrays of ordered helices).[39]

Therefore, the absorption area ratio 1000/1020 can be used as a descriptor of short-range order in the SNPs, since the ratio is expected to increase in systems with enhanced local formation of helices between dissolved starch chains following nanoprecipitation.

The 1050/1020 area ratio (Figures S2−S5, S8, and S10−S12), instead, is expected to increase in systems with extended arrays of ordered helices, i.e., for larger crystallinity increases. In our case, local order increases when the water content is raised in the nonsolvent blend up to a certain threshold value, and then decreases again for higher water content above the threshold. The same trends are obtained using ratios of bands' intensities at maxima or fwhm values (see Figure 2). We

https://doi.org/10.1021/acsami.4c02858
ACS Appl. Mater. Interfaces 2024, 16, 21185−21196

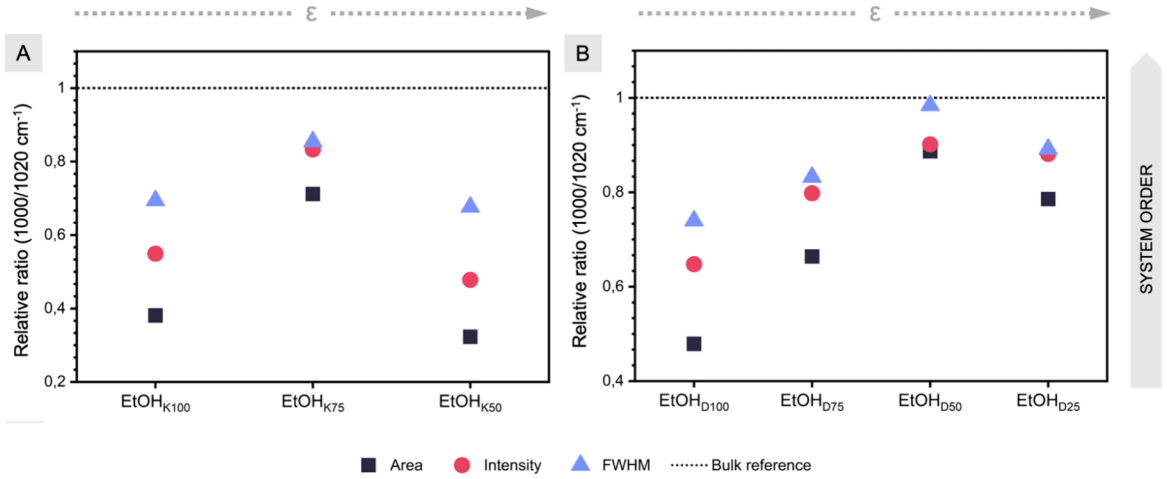

Figure 2. Short-range ordering of starch chains in SNPs produced through KOH (panel A) and DMSO (panel B) dissolution, followed by nonsolvent precipitation in different water/ethanol blends. The image shows variations in the ratio of areas (black squares), intensities (magenta circles), and full widths at half-maximum (fwhm) (blue triangles) between peaks at 1000 and 1020 cm^{-1} isolated via ATR-FTIR spectral band deconvolution. The data were normalized to the corresponding values of bulk Jin Shofu starch, and the SNPs are arranged along the *x*-axis with ascending values (from left to right) of the dielectric constant (ε) of the respective nonsolvents (water/ethanol blends) employed in the nanoprecipitation process. Errors are included in the markers.

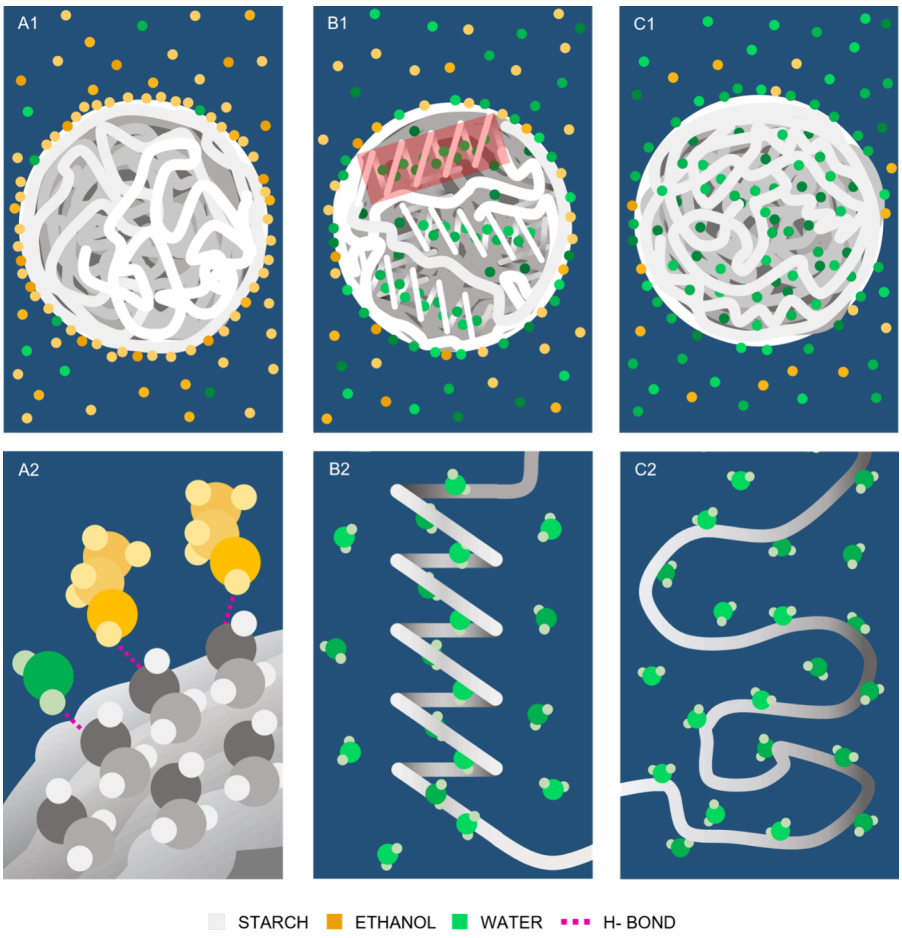

Figure 3. Schematic illustration of the possible interaction mechanisms between water/ethanol nonsolvent phases and starch chains as the water/ethanol ratio is varied. (A1, A2) At high ethanol content, some alcohol adsorption onto starch occurs, but the polymer chains remain undissolved and likely collapse abruptly in the nonsolvent, producing the observed amorphous particles. (B1, B2) Increasing water content, competition arises between for adsorption on starch. Water molecules, with a faster adsorption rate, initiate the formation of hydrogen bonds with starch, stabilizing the formation of local V-type helices (red highlight in panel B1) and thus local ordering that was observed experimentally. (C1, C2) At high water content, available sites on the polymer chains become saturated with water molecules; large water uptake can induce rapid transfer between the helical and coiled states, producing the measured decrease in local order.

https://doi.org/10.1021/acsami.4c02858
ACS Appl. Mater. Interfaces 2024, 16, 21185−21196

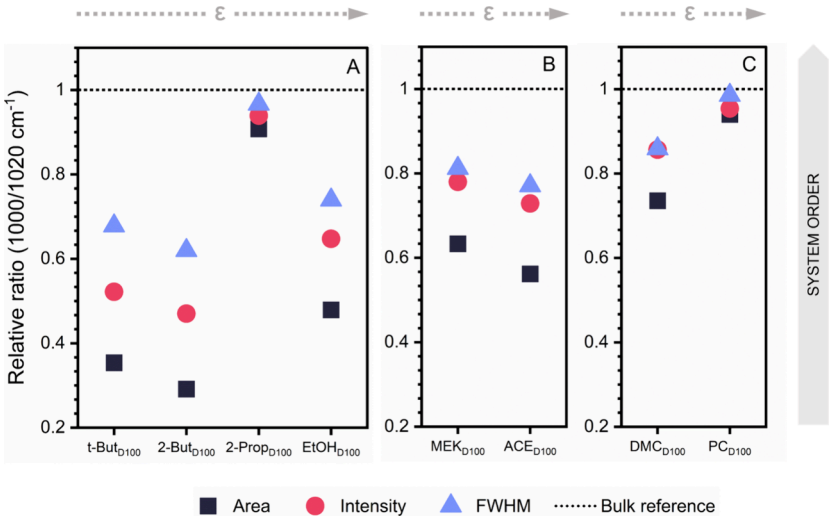

Figure 4. Short-range ordering of starch chains in SNPs produced through DMSO dissolution, followed by nonsolvent precipitation in different "green" solvents: alcohols (A), ketones (B), and alkyl carbonates (C). The image shows variations in the ratio of areas (black squares), intensities (magenta circles), and full widths at half-maximum (fwhm) (blue triangles) between peaks at 1000 and 1020 cm^{-1} isolated via Fourier spectral band deconvolution. The data were normalized to the corresponding values of bulk Jin Shofu starch, and the SNPs are arranged along the *x*-axis with ascending values (from left to right) of the dielectric constant (ε) of the respective nonsolvents (water/ethanol blends) employed in the nanoprecipitation process. Errors are included in the markers.

provide different possible hypotheses to explain these behaviors.

In the case of KOH dissolution before nanoprecipitation, local order increase by reduction of ethanol in the nonsolvent phase might be explained considering that, as the nonsolvent character of the precipitation blend is diminished, the dissolved starch chains experience a less abrupt assembly and can thus gain better organization. However, adding water in the nonsolvent also favors the partial migration of K^+ ions into the nonsolvent phase to which chains are exposed; these ions are known to be chaotropic,[49] and their effect seems to prevail when water content passes from 25 to 50%.

When nanoprecipitation follows dissolution in DMSO, the local order increases when water content is increased up to 50% and decreases passing to 75%. Because no chaotropic ions are present in this case, this trend could indicate a cononsolvency-like behavior of water with ethanol toward starch above a certain water content threshold. Cononsolvency has been shown to derive, in some cases, from differential uptake of solvents by the solute.[50] This could be the case here, considering differential uptake of water and ethanol by the starch polymers chains, a hypothesis supported by two known chemical behaviors reported by the literature, i.e., (1) the C6 site on starch glucose units is optimal for interaction with water,[51] but starch is also capable of giving secondary interactions (van der Waals, polar and H-bonding) with ethanol molecules;[52] (2) the adsorption rate of ethanol on starch is much slower than that of water.[52] At high ethanol content, the precipitation blend has full nonsolvent character, and low local order in the particles likely comes from abrupt chains assembly in a nonsolvent environment. Increasing water content, competition will start between water and ethanol for adsorption on starch:[52] water will start interacting with starch through hydrogen bonds, and water molecules have been shown to preserve helical conformation via H-bond bridging.[53] This known behavior could account for the partial recovery of local order (isolated helices), which we observed experimentally. However, upon further water addition to the solvent blend, the local order is lost again as shown in Figure 2. It is known from experimental and computational studies that starch polymer H-bonded helices are not stable in pure water, e.g., amylose chains can rapidly transfer between helical and coiled states on the order of 10−100s of nanoseconds,[54,55] and such fluid helix stability could produce the observed decrease in local order of the particles. A schematic illustration of these possible physicochemical mechanisms is provided in Figure 3.

In all cases, local ordering is not large enough to favor the self-assembly of extended arrays of helices, as demonstrated by the average flat trend of the IR 1050/1020 ratios in all systems, significantly lower than that of the bulk starch reference (see Figure S8).

Exposure of starch dissolved in KOH to an alternative set of green solvents (listed in Figure 1 and Table 2), other than water/ethanol blends or neat ethanol, led to the formation of macroscopic aggregates (millimeters; data not shown). On the other hand, dissolution in DMSO and exposure to the same solvents produced nanoprecipitation. The DLS analysis, after precipitation in the nonsolvents and dispersion in water, showed that the aqueous dispersions contain objects of ca. 170−260 nm (see Table 3). SEM analysis on the dried dispersions (see Figure S9) indicated sizes of ca. 40−50 nm, suggesting that small clusters of a few particles are present in the particles' aqueous dispersions (analyzed by DLS).

The IR 1050/1020 ratios are lower than bulk starch for almost all systems (see Figure S10), indicating that long-range order in starch polymer chains is not reestablished by nanoprecipitation, similarly to the SNPs produced by exposure to water/ethanol blends following DMSO or KOH dissolution. The SNPs precipitated in PC exhibit the highest ratio.

Instead, trends in the short-range ordering of starch chains emerged for classes of nonsolvents (see Figure 4 and Figures S11−S13). Nanoprecipitation in *t*-butanol and 2-butanol (the less polar alcohols in the pool) produced SNPs with the lowest local order among all of the tested solvents. Upon adsorption through the alcohol −OH termination onto starch chains, these molecules expose the bulky alkyl chains/groups and

https://doi.org/10.1021/acsami.4c02858
ACS Appl. Mater. Interfaces 2024, 16, 21185−21196

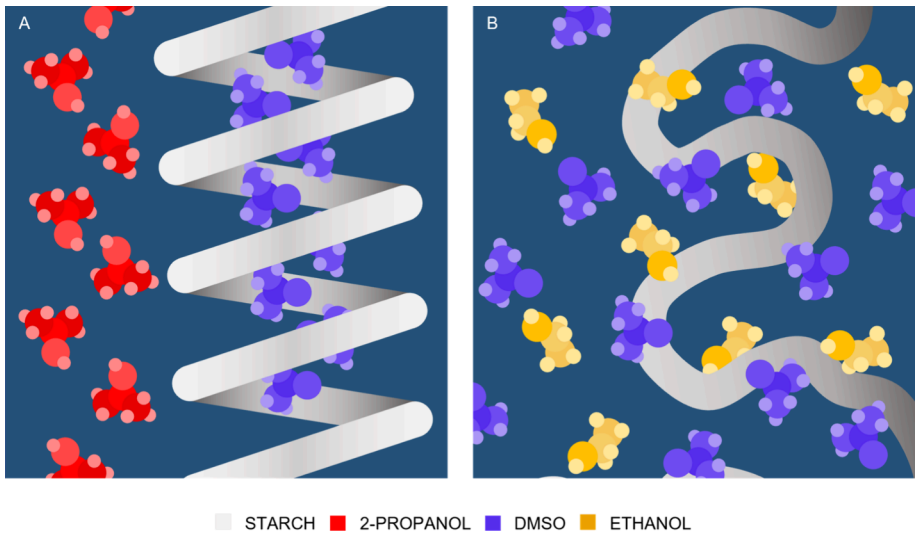

Figure 5. Visualization of possible changes in local starch order induced by known DMSO-alcohols and DMSO−starch interactions. (Panel A) The packing effect of 2-propanol dominates over heteroassociation with DMSO, leaving DMSO more accessible to starch; DMSO−starch interactions stabilize the local formation of starch helices (short-range ordering was here observed experimentally). (Panel B) Heteroassociation between ethanol and DMSO occurs through dipole−dipole interactions, reducing the availability of DMSO to stabilize the starch helices, which could produce the partial disruption of local ordering observed here experimentally.

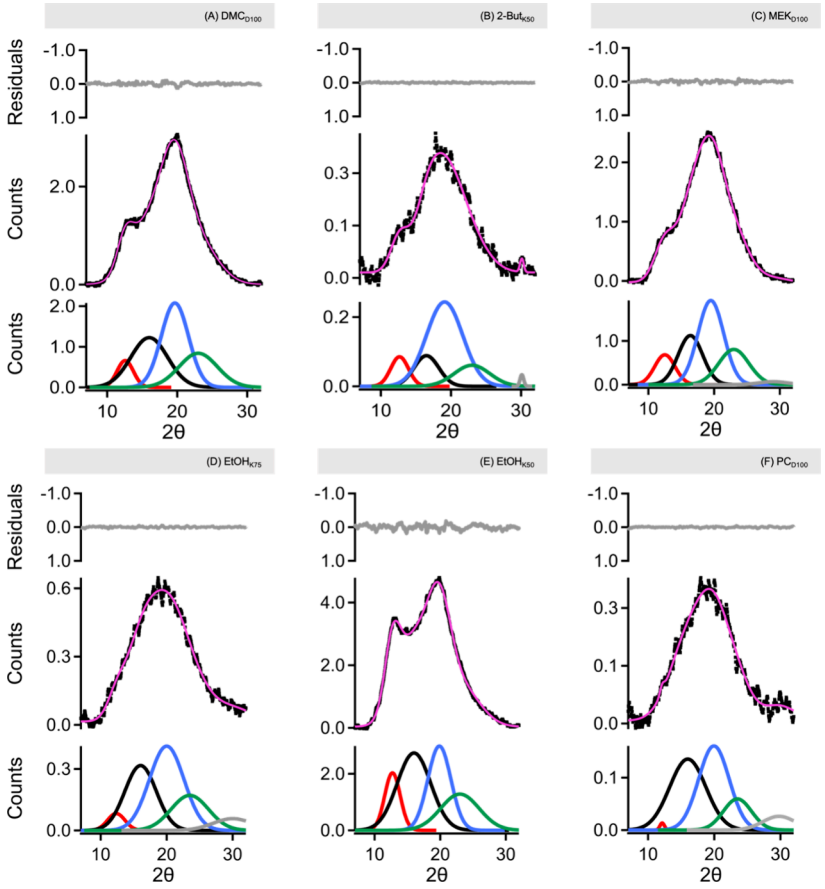

Figure 6. XRD spectra band deconvolution performed on six selected SNPs formulations that exhibited the widest range of short-range order as per ATR-FTIR analysis: (A) DMC_{D100}; (B) 2-But_{D100}; (C) MEK_{D100}; (D) $EtOH_{K75}$; (E) $EtOH_{K50}$; and (F) PC_{D100}. The diffraction region of interest spans from 7 to 36°. The *y*-axis represents the intensity of the Gaussian components (red, blue, green, gray, and black), experimental data (black dots), fitting curve (magenta line within the experimental data), and fitting residuals (light gray line above the diffractogram). The single helix components at ∼12.5 and ∼20° are highlighted in red and blue, respectively. The component related to double helices at ∼16° is depicted in black, while the B-type starch diffraction peak at ∼24° is shown in green.

https://doi.org/10.1021/acsami.4c02858
ACS Appl. Mater. Interfaces 2024, 16, 21185−21196

make the starch chains more hydrophobic. Thus, we hypothesize that the adsorbed butanol molecules could interfere with the formation of locally ordered H-bond networks (helices) between neighboring chains; the chains would then collapse abruptly in the nonsolvent phase with an overall mechanism resemblant of steric frustration in cononsolvency.[50] Indeed, increasing the polarity of the alcohol nonsolvent led to more local V-type structures in the SNPs. In particular, the use of 2-propanol produced the highest short-range order, which, however, is partially disrupted when ethanol is used (Figure 4). The latter effect could be ascribed to the different weak interactions that the two nonsolvents establish with DMSO during the nanoprecipitation procedure. Typically, DMSO-alcohol interactions get weaker as the size of the alcohol molecule increases, as demonstrated by changes in the excess molar volume of different DMS-alcohol blends.[56] Namely, while ethanol associates with DMSO through dipole−dipole interactions (heteroassociation), in the case of 2-propanol, self-association of pure components prevails over heteroassociation, in the so-called "packing effect".[56] These interactions reasonably affect the availability of DMSO molecules to interact with starch polymer chains. In turn, as reported in the literature, available DMSO molecules can stabilize the starch helix by interacting with only one hydroxyl group of the C-2 and C′-3 hydrogen bonded hydroxyl groups.[57] Thus, we hypothesized that changes in DMSO availability, regulated by different alcohols, could result in changes in local helix formation, and such a hypothesis is visualized in Figure 5. A similar trend is observed for ketones, passing from MEK to acetone. The larger MEK molecule likely gives more "packing effect" than heteroassociation with DMSO (more favored with acetone), leaving more DMSO available to stabilize isolated helices. Finally, in the case of alkyl carbonates, PC has a particularly high chemical affinity to DMSO thanks to the high dipole moments of the two molecules, favoring dipole−dipole and H-bonding interactions between the two solvents.[58] Such a high affinity could explain local order increase in the PC-precipitated SNPs, since less abrupt chain association during exposure to the nonsolvent should allow for some local order recovery in the precipitated SNPs, despite the lower availability of DMSO.

Additional and complementary insight on the effect of different nonsolvents (water/ethanol blends and neat green solvents) on the order of the SNPs was provided by XRD analysis of the particles after precipitation and drying. All the diffraction spectra show a broad band convolution between 10 and 30°, indicative of amorphous starch with scarce long-range packing of helices, and only a small diffraction peak at ∼23° possibly ascribable to B-type starch, which has less long-range order than A- or V-type.[59] Figure 6 shows the XRD profiles of six SNPs formulations whose short-range order (isolated helices), measured by ATR-FTIR and band deconvolution, ranges from the lowest, as in $EtOH_{K50}$, to the highest, as in PC_{D100}.

The features observed in the XRD profiles are consistent with the IR data, since they both point to significantly lower amounts of extended, long-range ordered packing of helices in the precipitated SNPs as opposed to bulk Jin Shofu starch, which instead was previously shown to exhibit the typical diffraction peaks of type A crystalline starch.[21] Gaussian deconvolution of the broad amorphous diffraction bands (Figure 6) gave information on the type of helices (single vs double) found in the amorphous structures for different SNPs formulations. According to the literature, the components at ∼12.5 and 19−20° are due to single helices, while that at ∼16° is due to double helices.[40] In all cases, the poorly packed structures contain preferentially single helices, and the largest gaps between single and double helices were found for SNPs precipitated in 2-butanol, MEK, and DMC. While it has been shown that looking for correlations between XRD and IR data on starch ordered structures can be misleading,[60] it must be noticed that the dominance of single over double helices is consistent with the presence of V-type isolated helices highlighted by ATR FTIR band deconvolution. The WAXS patterns of the same particles, which are less resolved than their XRD profiles, are indicative of largely amorphous samples (Figure S14), consistent with the XRD and IR data, confirming that no significant long-range ordered structures are present in the SNPs.

Overall, we conclude that starch crystallinity is lost during the dissolution phase, but the local order (isolated helices) can be recovered tuning the nature of the nonsolvent in the precipitation step. In particular, we have shown how the presence of V-type helices, usually low in state-of-the-art nanoprecipitation processes,[30,61] can be tuned using "green" nonsolvents with specific characteristics, which are known to give different physicochemical interactions with water, DMSO, and starch. This new approach is alternative, or complementary, to processes where starch crystallinity is regulated by factors such as the percentage of amylopectin and the length of polymer chains.[62]

When aqueous dispersions of the obtained SNPs were applied on powdery paints, the cohesion between the weakly bound pigments was effectively achieved, producing mechanically stable layers through a feasible applicative protocol. Namely, cohesion increases significantly, leading to a consolidation efficacy of ∼99%, as measured through semi-quantitative evaluation of pigment removal before and after treatment with the SNPs (Figure S15). Acceptable consolidation could be achieved also with particles with lower local order before dispersion in water, indicating that the choice of synthetic routes can be mainly dictated by sustainability (lower water consumption or lower costs) and safety/upscalability (lower solvent's flammability or ecotoxicological impact). Moreover, no aesthetic alteration was induced on the treated paints by application of the SNPs (Figure S16), while treatment with dispersions of bulk starch was previously shown to yield glossy surface layers that jeopardize the matte aspect of the painted layers.[21] These results validate the new synthetic nanoprecipitation approaches as valuable routes to formulate alternative "green" consolidants for painting conservation, aiming to replace bulk starch and synthetic adhesives in traditional restoration practice.

CONCLUSIONS

We studied the effects of nonsolvency on the precipitation of starch nanoparticles (SNPs), using dissolution of Jin Shofu starch in alkali (KOH) or DMSO, and a set of "green" nonsolvents with different physicochemical characteristics. Dissolution in DMSO opens to the use of a wide spectrum of "green" nonsolvents to obtain the SNPs, while only water−ethanol blends gave effective nanoprecipitation following dissolution in KOH. Interestingly, we demonstrated here for the first time how the local order in SNPs (e.g., formation of isolated V-type helices) can be tuned by selecting "green" nonsolvents with different properties, including alcohols,

https://doi.org/10.1021/acsami.4c02858
ACS Appl. Mater. Interfaces 2024, 16, 21185−21196

ketones, and alkyl carbonates. This is a significant advancement in the nanoprecipitation of amorphous starch assemblies, which is still largely unexplored.

Variations in the short-range (molecular) order were observed, with specific trends for different nonsolvents used in the nanoprecipitation. Following dissolution in DMSO, the presence of water in blends with ethanol favors the ordering of starch, but over a certain threshold, water exhibits a cononsolvency-like behavior inducing an order decrease. This was ascribed to progressive water saturation of adsorption sites in the chains, where water molecules progressively act as stabilizers of helices via H-bonding[53] and then favor helix−coil transitions in starch polymers.[54,55] In the case of KOH dissolution, an order decrease over a certain water content was explained considering that water addition also introduces chaotropic K^+ ions in the starch assemblies. When DMSO dissolution is followed by exposure to the other "green" nonsolvents, local order variations in the SNPs could be explained by known mechanisms like steric frustration, heteroassociation or "packing effect" between DMSO and the nonsolvents.[56] Moreover, enhancing the nonsolvent character of the precipitation compound/blend likely causes abrupt assembly and thus order decrease in the polymer chains.

Overall, we showed how local order can be recovered and tuned in dissolved starch by exposure to different "green" nonsolvents, while long-range order (extended arrays of helices) is poor, as shown by X-ray diffraction and WAXS measurements. Aqueous dispersions of the obtained SNPs produced effective consolidation of decohered paint layers without aesthetic alterations. Acceptable consolidation is achieved also with particles with lower local order before dispersion in water, indicating that the choice of synthetic routes can be mainly dictated by sustainability (lower water consumption or lower costs) and safety and scalability (lower flammability or ecotoxicological impact). The proposed SNP formulations candidate as valuable consolidants for canvas and easel paintings, alternative to bulk starch dispersions or detrimental synthetic adhesives, and complement inorganic particles or nanocomposites previously formulated for the consolidation and protection or works of art.[6,21,26,63−67] In addition, the possibility of feasibly tuning local order in the amorphous SNPs can positively affect fields like food chemistry, industrial packaging, pharmaceutics, drug delivery, nutraceuticals, and nanocomposites, where the use of amorphous starch with controlled physicochemical properties, rather than starch nanocrystals, has potential impact in numerous applications.[24,68,69]

■ ASSOCIATED CONTENT

Supporting Information

The Supporting Information is available free of charge at https://pubs.acs.org/doi/10.1021/acsami.4c02858.

Calculation of solubility and interaction parameters; SEM images of the dried starch formulations; STEM images of SNPs water dispersions; correlation functions of SNP aqueous dispersions, from DLS; additional FTIR ATR analysis of short-range and long-range ordering and of starch chains in SNPs produced through KOH and DMSO dissolution, followed by nonsolvent precipitation in different water/ethanol blends and pure "green" solvents; ATR-FTIR spectra of the SNPs and band deconvolutions; WAXS profiles of the dried SNPs; macro photographs of ultramarine blue paint mock-ups before and after treatment with Jin Shofu starch SNPs; and comparison of image analysis results between macro photographs of fiberglass filters after contact with the ultramarine blue aged mock-ups (PDF)

■ AUTHOR INFORMATION

Corresponding Author

David Chelazzi − *Department of Chemistry "Ugo Schiff" and CSGI, University of Florence, Florence I-50019, Italy;* orcid.org/0000-0001-9994-3356; Email: david.chelazzi@unifi.it

Authors

Andrea Casini − *CSGI and Department of Chemistry "Ugo Schiff", University of Florence, Florence I-50019, Italy;* orcid.org/0000-0003-4256-8887

Margherita Casagli − *Department of Chemistry "Ugo Schiff" and CSGI, University of Florence, Florence I-50019, Italy*

Giovanna Poggi − *Department of Chemistry "Ugo Schiff" and CSGI, University of Florence, Florence I-50019, Italy;* orcid.org/0000-0002-4158-0705

Piero Baglioni − *CSGI and Department of Chemistry "Ugo Schiff", University of Florence, Florence I-50019, Italy;* orcid.org/0000-0003-1312-8700

Complete contact information is available at: https://pubs.acs.org/10.1021/acsami.4c02858

Author Contributions

Conceptualization and design were done by DC., A.C., and P.B.; A.C., M.C., DC., and G.P. conducted the experiments; and all authors analyzed the experimental data. D.C. and P.B. supervised the experiments; writing—original draft—was done by DC., A.C., and G.P. Writing—review and editing—was done by D.C., A.C., G.P., and P.B. All authors have given approval to the final version of the manuscript.

Funding

A.C., D.C, G.P., and P.B. received funding from CSGI (CMPT191138 MUR) and the EU (HORIZON EUROPE GREENART, grant agreement 101060941).

Notes

The authors declare no competing financial interest.

■ ACKNOWLEDGMENTS

This project has received fundings from CSGI (Consorzio per lo Sviluppo dei Sistemi a Grande Interfase, Center for Colloid and Surface Science) and from the European project GREENART (GREen ENdeavor in Art ResToration) under the Horizon Europe Grant Agreement 101060941. Views and opinions expressed are however those of the author(s) only and do not necessarily reflect those of the European Union or the European Research Executive Agency (REA). Neither the European Union nor the granting authority can be held responsible for them. Antonio Mirabile (paper conservator) is gratefully acknowledged for providing the Jin Shofu starch. Dr. Laura Capozzoli (CNR CEME) is gratefully acknowledged for assistance in the STEM images acquisition.

REFERENCES

(1) Zimmerman, J. B.; Anastas, P. T.; Erythropel, H. C.; Leitner, W. Designing for a Green Chemistry Future. *Science* **2020**, *367* (6476), 397−400.

(2) Boccaccini, F.; Giuliani, C.; Pascucci, M.; Riccucci, C.; Messina, E.; Staccioli, M. P.; Ingo, G. M.; Di Carlo, G. Toward a Green and Sustainable Silver Conservation: Development and Validation of Chitosan-Based Protective Coatings. *Int. J. Mol. Sci.* **2022**, *23* (22), 14454.

(3) Poggi, G.; Santan, H. D.; Smets, J.; Chelazzi, D.; Noferini, D.; Petruzzellis, M. L.; Pensabene Buemi, L.; Fratini, E.; Baglioni, P. Nanostructured Bio-Based Castor Oil Organogels for the Cleaning of Artworks. *J. Colloid Interface Sci.* **2023**, *638*, 363−374.

(4) Camargos, C. H. M.; Poggi, G.; Chelazzi, D.; Baglioni, P.; Rezende, C. A. Protective Coatings Based on Cellulose Nanofibrils, Cellulose Nanocrystals, and Lignin Nanoparticles for the Conservation of Cellulosic Artifacts. *ACS Appl. Nano Mater.* **2022**, *5* (9), 13245−13259.

(5) Baglioni, P.; Chelazzi, D. How Science Can Contribute to the Remedial Conservation of Cultural Heritage. *Eur. J. Chem.* **2021**, *27* (42), 10798−10806.

(6) Cianci, C.; Chelazzi, D.; Poggi, G.; Modi, F.; Giorgi, R.; Laurati, M. Hybrid Fibroin-Nanocellulose Composites for the Consolidation of Aged and Historical Silk. *Colloids Surf. A: Physicochem* **2022**, *634*, No. 127944.

(7) Stjerndahl, M.; Lundberg, D.; Chauhan, V.; Bordes, R.; Holmberg, K. Cleavable Surfactants: A Comparison between Ester, Amide, and Carbonate as the Weak Bond. *JSD* **2019**, *22* (5), 1139−1145.

(8) Passaretti, A.; Cuvillier, L.; Sciutto, G.; Guilminot, E.; Joseph, E. Biologically Derived Gels for the Cleaning of Historical and Artistic Metal Heritage. *Appl. Sci.* **2021**, *11* (8), 3405.

(9) Prati, S.; Volpi, F.; Fontana, R.; Galletti, P.; Giorgini, L.; Mazzeo, R.; Mazzocchetti, L.; Samorì, C.; Sciutto, G.; Tagliavini, E. Sustainability in Art Conservation: A Novel Bio-Based Organogel for the Cleaning of Water Sensitive Works of Art. *Pure Appl. Chem.* **2018**, *90* (2), 239−251.

(10) Rosciardi, V.; Chelazzi, D.; Baglioni, P. Green" Biocomposite Poly (Vinyl Alcohol)/Starch Cryogels as New Advanced Tools for the Cleaning of Artifacts. *J. Colloid Interface Sci.* **2022**, *613*, 697−708.

(11) Zuliani, A.; Chelazzi, D.; Mastrangelo, R.; Giorgi, R.; Baglioni, P. Adsorption Kinetics of Acetic Acid into ZnO/Castor Oil-Derived Polyurethanes. *J. Colloid Interface Sci.* **2023**, *632*, 74−86.

(12) Zuliani, A.; Bandelli, D.; Chelazzi, D.; Giorgi, R.; Baglioni, P. Environmentally Friendly ZnO/Castor Oil Polyurethane Composites for the Gas-Phase Adsorption of Acetic Acid. *J. Colloid Interface Sci.* **2022**, *614*, 451−459.

(13) Gueidão, M.; Vieira, E.; Bordalo, R.; Moreira, P. Available Green Conservation Methodologies for the Cleaning of Cultural Heritage: An Overview. *Estudos Conservação Restauro* **2020**, *12*, 22−44.

(14) Prat, D.; Wells, A.; Hayler, J.; Sneddon, H.; McElroy, C. R.; Abou-Shehada, S.; Dunn, P. J. CHEM21 Selection Guide of Classical- and Less Classical-Solvents. *RSC Green Chem.* **2016**, *18* (1), 288−296.

(15) Casini, A.; Chelazzi, D.; Baglioni, P. Advanced Methodologies for the Cleaning of Works of Art. *Sci. China Technol. Sci.* **2023**, *66*, 2162.

(16) Sfameni, S.; Rando, G.; Plutino, M. R. Sustainable Secondary-Raw Materials, Natural Substances and Eco-Friendly Nanomaterial-Based Approaches for Improved Surface Performances: An Overview of What They Are and How They Work. *Int. J. Mol. Sci.* **2023**, *24* (6), 5472.

(17) Haaj, S. B.; Thielemans, W.; Magnin, A.; Boufi, S. Starch Nanocrystal Stabilized Pickering Emulsion Polymerization for Nanocomposites with Improved Performance. *ACS Appl. Mater. Interfaces* **2014**, *6* (11), 8263−8273.

(18) Kierulf, A.; Enayati, M.; Yaghoobi, M.; Whaley, J.; Smoot, J.; Perez Herrera, M.; Abbaspourrad, A. Starch Janus Particles: Bulk Synthesis, Self-Assembly, Rheology, and Potential Food Applications. *ACS Appl. Mater. Interfaces* **2022**, *14* (51), 57371−57386.

(19) Kaushal, A. M.; Gupta, P.; Bansal, A. K. Amorphous Drug Delivery Systems: Molecular Aspects, Design, and Performance. *Crit. Rev. Ther. Drug Carr.* **2004**, *21* (3), 133−193.

(20) Joye, I. J. Starch. In *Encyclopedia of Food Chemistry*; Melton, L. D., Shahidi, F., Varelis, P., Eds.; Academic Press: Oxford, 2019; pp 256−264. DOI: 10.1016/B978-0-08-100596-5.21586-2.

(21) Casini, A.; Chelazzi, D.; Giorgi, R. Jin Shofu Starch Nanoparticles for the Consolidation of Modern Paintings. *ACS Appl. Mater. Interfaces* **2021**, 37924.

(22) Phothisarattana, D.; Wongphan, P.; Promhuad, K.; Promsorn, J.; Harnkarnsujarit, N. Biodegradable Poly(Butylene Adipate-Co-Terephthalate) and Thermoplastic Starch-Blended TiO2 Nanocomposite Blown Films as Functional Active Packaging of Fresh Fruit. *Polymers* **2021**, *13* (23), 4192.

(23) Plucinski, A.; Lyu, Z.; Schmidt, B. V. K. J. Polysaccharide Nanoparticles: From Fabrication to Applications. *J. Mater. Chem. B* **2021**, *9* (35), 7030−7062.

(24) Le Corre, D.; Bras, J.; Dufresne, A. Starch Nanoparticles: A Review. *Biomacromolecules* **2010**, *11* (5), 1139−1153.

(25) Hassan, N. A.; Darwesh, O. M.; Smuda, S. S.; Altemimi, A. B.; Hu, A.; Cacciola, F.; Haoujar, I.; Abedelmaksoud, T. G. Recent Trends in the Preparation of Nano-Starch Particles. *Molecules* **2022**, *27* (17), 5497.

(26) Chelazzi, D.; Chevalier, A.; Pizzorusso, G.; Giorgi, R.; Menu, M.; Baglioni, P. Characterization and Degradation of Poly(Vinyl Acetate)-Based Adhesives for Canvas Paintings. *Polym. Degrad.* **2014**, *107*, 314−320.

(27) Ge, S.; Xiong, L.; Li, M.; Liu, J.; Yang, J.; Chang, R.; Liang, C.; Sun, Q. Characterizations of Pickering Emulsions Stabilized by Starch Nanoparticles: Influence of Starch Variety and Particle Size. *Food Chem.* **2017**, *234*, 339−347.

(28) Angioloni, A.; Collar, C. Small and Large Deformation Viscoelastic Behaviour of Selected Fibre Blends with Gelling Properties. *Food Hydrocoll.* **2009**, *23* (3), 742−748.

(29) Zhu, F. Interactions between Starch and Phenolic Compound. *Food Sci. Technol.* **2015**, *43* (2), 129−143.

(30) Javidi, F.; Razavi, S. M. A.; Mohammad Amini, A. Cornstarch Nanocrystals as a Potential Fat Replacer in Reduced Fat O/W Emulsions: A Rheological and Physical Study. *Food Hydrocoll.* **2019**, *90*, 172−181.

(31) Ding, Y.; Zheng, J.; Zhang, F.; Kan, J. Synthesis and Characterization of Retrograded Starch Nanoparticles through Homogenization and Miniemulsion Cross-Linking. *Carbohydr.* **2016**, *151*, 656−665.

(32) Karg, M.; Pich, A.; Hellweg, T.; Hoare, T.; Lyon, L. A.; Crassous, J. J.; Suzuki, D.; Gumerov, R. A.; Schneider, S.; Potemkin, I. I.; Richtering, W. Nanogels and Microgels: From Model Colloids to Applications, Recent Developments, and Future Trends. *Langmuir* **2019**, *35* (19), 6231−6255.

(33) Amigo, N.; Palza, H.; Canales, D.; Sepúlveda, F.; Vasco, D. A.; Sepúlveda, F.; Zapata, P. A. Effect of Starch Nanoparticles on the Crystallization Kinetics and Photodegradation of High Density Polyethylene. *Composites, Part B* **2019**, *174*, No. 106979.

(34) Provencher, S. W. CONTIN: A General Purpose Constrained Regularization Program for Inverting Noisy Linear Algebraic and Integral Equations. *Comput. Phys. Commun.* **1982**, *27* (3), 229−242.

(35) Rueden, C. T.; Schindelin, J.; Hiner, M. C.; DeZonia, B. E.; Walter, A. E.; Arena, E. T.; Eliceiri, K. W. ImageJ2: ImageJ for the next Generation of Scientific Image Data. *BMC Bioinform.* **2017**, *18* (1), 529.

(36) Legland, D.; Arganda-Carreras, I.; Andrey, P. MorphoLibJ: Integrated Library and Plugins for Mathematical Morphology with ImageJ. *Bioinformatics* **2016**, *32* (22), 3532−3534.

(37) Chinga, G.; Syverud, K. Quantification of Paper Mass Distributions within Local Picking Areas. *Nord. Pulp Pap. Res. J.* **2007**, *22* (4), 441−446.

https://doi.org/10.1021/acsami.4c02858
ACS Appl. Mater. Interfaces 2024, 16, 21185−21196

(38) Warren, F. J.; Gidley, M. J.; Flanagan, B. M. Infrared Spectroscopy as a Tool to Characterise Starch Ordered Structure - A Joint FTIR-ATR, NMRXRD and DSC Study. *Carbohydr. Polym.* **2016**, *139*, 35−42.
(39) van Soest, J. J. G.; De Wit, D.; Tournois, H.; Vliegenthart, J. F. G. Retrogradation of Potato Starch as Studied by Fourier Transform Infrared Spectroscopy. *Stärke* **1994**, *46* (12), 453−457.
(40) Bayer, R. K.; Cagiao, M. E.; Calleja, F. J. B. Structure Development in Amorphous Starch as Revealed by X-Ray Scattering: Influence of the Network Structure and Water Content. *J. Appl. Polym. Sci.* **2006**, *99* (4), 1880−1886.
(41) Buléon, A.; Colonna, P.; Planchot, V.; Ball, S. Starch Granules: Structure and Biosynthesis. *Int. J. Biol. Macromol.* **1998**, *23* (2), 85−112.
(42) Macchiagodena, M.; Bassu, G.; Vettori, I.; Fratini, E.; Procacci, P.; Pagliai, M. 2-Butanol Aqueous Solutions: A Combined Molecular Dynamics and Small/Wide-Angle X-Ray Scattering Study. *J. Phys. Chem. A* **2022**, *126* (47), 8826−8833.
(43) Mattox, T. M.; Urban, J. J. Tuning the Surface Plasmon Resonance of Lanthanum Hexaboride to Absorb Solar Heat: A Review. *Materials* **2018**, *11* (12), 2473.
(44) Byrne, F. P.; Jin, S.; Paggiola, G.; Petchey, T. H. M.; Clark, J. H.; Farmer, T. J.; Hunt, A. J.; Robert McElroy, C.; Sherwood, J. Tools and Techniques for Solvent Selection: Green Solvent Selection Guides. *Sustain. Chem. Process.* **2016**, *4* (1), 1−24.
(45) Venturi, D. M.; Campana, F.; Marmottini, F.; Costantino, F.; Vaccaro, L. Extensive Screening of Green Solvents for Safe and Sustainable UiO-66 Synthesis. *ACS Sustainable Chem. Eng.* **2020**, *8* (46), 17154−17164.
(46) Fessi, H.; Puisieux, F.; Devissaguet, J. Ph.; Ammoury, N.; Benita, S. Nanocapsule Formation by Interfacial Polymer Deposition Following Solvent Displacement. *Int. J. Pharm.* **1989**, *55* (1), R1−R4.
(47) Tan, Y.; Xu, K.; Li, L.; Liu, C.; Song, C.; Wang, P. Fabrication of Size-Controlled Starch-Based Nanospheres by Nanoprecipitation. *ACS Appl. Mater. Interfaces* **2009**, *1* (4), 956−959.
(48) Wu, X.; Chang, Y.; Fu, Y.; Ren, L.; Tong, J.; Zhou, J. Effects of Non-Solvent and Starch Solution on Formation of Starch Nanoparticles by Nanoprecipitation. *Stärke* **2016**, *68* (3−4), 258−263.
(49) Sripa, P.; Tongraar, A.; Kerdcharoen, T. Characteristics of K+ and Rb+ as "Structure-Breaking" Ions in Dilute Aqueous Solution: Insights from ONIOM-XS MD Simulations. *Chem. Phys.* **2016**, *479*, 72−80.
(50) Bharadwaj, S.; Niebuur, B.-J.; Nothdurft, K.; Richtering, W.; van der Vegt, N. F. A.; Papadakis, C. M. Cononsolvency of Thermoresponsive Polymers: Where We Are Now and Where We Are Going. *Soft Matter* **2022**, *18* (15), 2884−2909.
(51) Panić, V. V.; Šešlija, S. I.; Nešić, A. R.; Veličković, S. J. Adsorption of Azo Dyes on Polymer Materials. *Hemijska industrija* **2013**, *67* (6), 881−900.
(52) Lee, J. Y.; Westgate, P. J.; Ladisch, M. R. Water and Ethanol Sorption Phenomena on Starch. *AIChE J.* **1991**, *37* (8), 1187−1195.
(53) Naidoo, K. J.; Kuttel, M. Water Structure about the Dimer and Hexamer Repeat Units of Amylose from Molecular Dynamics Computer Simulations. *J. Comput. Chem.* **2001**, *22* (4), 445−456.
(54) Khatami, M. H.; Barber, W.; de Haan, H. W. Using Geometric Criteria to Study Helix-like Structures Produced in Molecular Dynamics Simulations of Single Amylose Chains in Water. *RSC Adv.* **2021**, *11* (20), 11992−12002.
(55) Zhang, Q.; Lu, Z.; Hu, H.; Yang, W.; Marszalek, P. E. Direct Detection of the Formation of V-Amylose Helix by Single Molecule Force Spectroscopy. *J. Am. Chem. Soc.* **2006**, *128* (29), 9387−9393.
(56) Palaiologou, M. M.; Arianas, G. K.; Tsierkezos, N. G. Thermodynamic Investigation of Dimethyl Sulfoxide Binary Mixtures at 293.15 and 313.15 K. *J. Solution Chem.* **2006**, *35* (11), 1551−1565.
(57) Erlander, S. R.; Tobin, R. The Stability of the Helix of Amylose and Amylopectin in DMSO and Water Solutions. *Makromol. Chem.* **1968**, *111* (1), 194−211.
(58) Koverga, V. A.; Voroshylova, I. V.; Smortsova, Y.; Miannay, F.-A.; Cordeiro, M. N. D. S.; Idrissi, A.; Kalugin, O. N. Local Structure and Hydrogen Bonding in Liquid γ-Butyrolactone and Propylene Carbonate: A Molecular Dynamics Simulation. *J. Mol. Liq.* **2019**, *287*, No. 110912.
(59) Dome, K.; Podgorbunskikh, E.; Bychkov, A.; Lomovsky, O. Changes in the Crystallinity Degree of Starch Having Different Types of Crystal Structure after Mechanical Pretreatment. *Polymers* **2020**, *12* (3), 641.
(60) Sevenou, O.; Hill, S. E.; Farhat, I. A.; Mitchell, J. R. Organisation of the External Region of the Starch Granule as Determined by Infrared Spectroscopy. *Int. J. Biol. Macromol.* **2002**, *31* (1), 79−85.
(61) Wang, F.; Chang, R.; Ma, R.; Tian, Y. Eco-Friendly and Superhydrophobic Nano-Starch Based Coatings for Self-Cleaning Application and Oil-Water Separation. *Carbohydr.* **2021**, *271*, No. 118410.
(62) Suriya, M.; Reddy, C. K.; Haripriya, S.; Harsha, N. Influence of Debranching and Retrogradation Time on Behavior Changes of Amorphophallus Paeoniifolius Nanostarch. *Int. J. Biol. Macromol.* **2018**, *120*, 230−236.
(63) Olivieri, F.; Castaldo, R.; Cocca, M.; Gentile, G.; Lavorgna, M. Mesoporous Silica Nanoparticles as Carriers of Active Agents for Smart Anticorrosive Organic Coatings: A Critical Review. *Nanoscale* **2021**, *13* (20), 9091−9111.
(64) Barberio, M.; Veltri, S.; Imbrogno, A.; Stranges, F.; Bonanno, A.; Antici, P. TiO2 and SiO2 Nanoparticles Film for Cultural Heritage: Conservation and Consolidation of Ceramic Artifacts. *Surf. Coat.* **2015**, *271*, 174−180.
(65) Camerini, R.; Chelazzi, D.; Giorgi, R.; Baglioni, P. Hybrid Nano-Composites for the Consolidation of Earthen Masonry. *J. Colloid Interface Sci.* **2019**, *539*, 504−515.
(66) Chelazzi, D.; Giorgi, R.; Baglioni, P. Nanotechnology for Vasa Wood De-Acidification. *Macromol. Symp.* **2006**, *238* (1), 30−36.
(67) Giorgi, R.; Chelazzi, D.; Fratini, E.; Langer, S.; Niklasson, A.; Rådemar, M.; Svensson, J.-E.; Baglioni, P. Nanoparticles of Calcium Hydroxide for Wood Deacidification: Decreasing the Emissions of Organic Acid Vapors in Church Organ Environments. *J. Cult. Herit.* **2009**, *10* (2), 206−213.
(68) Torres, F. G.; De-la-Torre, G. E. Synthesis, Characteristics, and Applications of Modified Starch Nanoparticles: A Review. *Int. J. Biol. Macromol.* **2022**, *194*, 289−305.
(69) Campelo, P. H.; Sant'Ana, A. S.; Pedrosa Silva Clerici, M. T. Starch Nanoparticles: Production Methods, Structure, and Properties for Food Applications. *Curr. Opin. Food Sci.* **2020**, *33*, 136−140.

https://doi.org/10.1021/acsami.4c02858
ACS Appl. Mater. Interfaces 2024, 16, 21185−21196